Molecular Beamforming for Actuation in Molecular Communication Networks

Joana Angjo, Ali E. Pusane, *Senior Member, IEEE*, H. Birkan Yilmaz, *Member, IEEE*, Ertugrul Basar, *Fellow, IEEE*, and Tuna Tugcu, *Senior Member, IEEE*

***Abstract*— The actuation accuracy of sensing tasks performed by molecular communication (MC) schemes is a very important metric. Reducing the effect of sensors fallibility can be achieved by improvements and advancements in the sensor and communication networks design. Inspired by the technique of beamforming used extensively in radio frequency communication systems, a novel molecular beamforming design is proposed in this paper. This design can find application in tasks related to actuation of nano machines in MC networks. The main idea behind the proposed scheme is that the utilization of more sensing nano machines in a network can increase the overall accuracy of that network. In other words, the probability of an actuation error reduces as the number of sensors that collectively take the actuation decision increases. In order to achieve this, several design procedures are proposed. Three different scenarios for the observation of the actuation error are investigated. For each case, the analytical background is provided and compared with the results obtained by computer simulations. The improvement in the actuation accuracy by means of molecular beamforming is verified for a uniform linear array as well as for a random topology.**

***Index Terms*— Molecular beamforming, molecular communication, actuation.**

I. Introduction

DUE to its high potential with regard to the realization of communication on a small scale, the nanonetworking paradigm has received increased attention in recent years [1]. Considering that small scale communication is characterized by constraints that make electromagnetic communication infeasible, researchers have focused their attention on molecular communications (MC). The idea behind MC is that, unlike traditional communication systems that utilize radio frequency (RF) signals, the information is carried by the wave of molecules. Molecules are released by the transmitter nanomachine, and they propagate in the environment according to their and the surrounding medium's characteristics towards the receiver nanomachine, which decodes the information from the properties of the molecular wave [2]. Numerous systems have been proposed in the literature, among which molecular communication via diffusion (MCvD) is the most promising one, as a result of its high energy efficiency and low complexity [3]. The diffusive nature of the molecules is utilized in MCvD systems for information transmission.

Nano communication offers a vast set of prospective applications in fields such as medicine and healthcare. As stated in [4], nano communication technologies enable noninvasive solutions for in-body sensing and actuation, which can clearly enhance the processes of diagnosis and treatment of various health related issues. One of the advantages of using MC for medical therapies is its capability to prevent side effects [5]. A number of applications have been proposed in the literature, starting from disease detection to treatment by using targeted drug delivery, immune system triggering, nanosurgery [6], [7], [8], [9]. For example, a discussion about the treatment of diabetes by means of nanotechnology is given in [10]. Recent studies propose that the level of glucose can be constantly measured by means of *in vivo* sensors, and responses to changes in the level can be made possible through novel advancements in insulin delivery systems.

Small scale communication is highly related to the progression and development of sensors. Sensors play a crucial role in collecting data, which is essential for monitoring and analysing a specific environment. For instance, the authors of [7] propose a network that may be used to detect circulating tumoral cells, which basically relies on mobile sensors that store information whenever a tumor cell is encountered in the circulatory system. In [11], the authors analyse the impact of the integration of nano sensors with big data and the benefits that follow when applied to healthcare applications. The sensing accuracy of these sensors is a very decisive parameter, especially when used for applications related to human health. There are parameters in the literature for measuring the accuracy of nano sensors. For example, evaluation of glucose biosensors in terms of spectral response, linearity, sensitivity, limit of detection, kinetic response, reversibility, stability, precision, and accuracy is proposed in [12]. This study evaluates its results in accordance with the regulations given in [13]. Similarly, the authors of [14] investigate the accuracy and stability of a biosensor used to monitor arterial glucose. As expected,

Manuscript received 26 October 2022; revised 25 February 2023 and 28 April 2023; accepted 30 June 2023. Date of publication 4 July 2023; date of current version 3 January 2024. This work was supported in part by the Scientific and Technical Research Council of Turkey (TUBITAK) under Grant 119E190. *(Corresponding author: Joana Angjo.)*

Joana Angjo and Ertugrul Basar are with the Department of Electrical and Electronics Engineering, Koç University, 34450 İstanbul, Turkey (e-mail: jangjo20@ku.edu.tr; ebasar@ku.edu.tr).

Ali E. Pusane is with the Department of Electrical and Electronics Engineering, Boğaziçi University, 34342 İstanbul, Turkey (e-mail: ali.pusane@boun.edu.tr).

H. Birkan Yilmaz and Tuna Tugcu are with the Department of Computer Engineering, Boğaziçi University, 34342 İstanbul, Turkey (e-mail: birkan.yilmaz@boun.edu.tr; tugcu@boun.edu.tr).

Digital Object Identifier 10.1109/TNB.2023.3292131

errors are quite possible in real-time applications. Attempts to increase the accuracy of nano systems can be made in terms of nano sensors design and system implementation.

A. Related Works

There are several works in the literature focusing on cooperative sensing for improving the accuracy when the sensors are imperfect. The idea behind cooperation between nano sensors for triggering a collective response is exemplified in [15], where the authors discuss how bio-nano sensor networks can revolutionize healthcare systems. For example, the authors of [16] focus on both abnormality detection and localization in fluidic mediums, achieved by cooperative activation of several mobile sensors. They conclude that the detection performance enhances due to the collaboration between the sensors for activating each other. Similar results are obtained in [17], where the authors propose target detection via several receptors distributed in a tissue. When a target is present and encountered by these receptors, they get activated and react in notifying about the presence of the target. In this study, the reactive nanosensors get actuated when they encounter some specific biomarkers, and they release some other type of molecules which travel towards a fusion center, where the final decision about the presence of a target is made. The probability of missed detection versus the probability of a false alarm is evaluated as well. The idea of joint detection is also studied in [18], where the decision for the localization of an abnormality is performed by a gateway device based on the information received from multiple fusion centers. In this work, the sensors are considered to be mobile and they release molecules once they are activated, which are then received by the fusion centers. The results show that the probability of localization error drops as the number of released molecules increases. The authors of [19] focus on abnormality detection by several cooperative mobile nanomachines, where the final decision is made by applying OR and AND logic-based fusion rules by the mobile fusion center. A study aiming early cancer detection using mobile sensors is proposed in [20], for which the authors derive two different detectors for the decision making at the fusion center, where the sensors that are activated once they detect cancer biomarkers are collected. Similarly, biomarkers' concentration for anomaly detection by using MC is studied in [21]. Meanwhile, the authors of [22] study cooperative networks consisting of one transmitter and several receiver nodes, and they perform symbol-by-symbol maximum likelihood detection at the fusion center for choosing the most likely transmitted signal.

Parallel to the advancements in RF communication systems, novel designs on the small scale levels have been proposed in order to overcome challenges that are faced by these systems and enhance their performance. For instance, authors of [23] propose several detection algorithms for a multiple-input multiple-output (MIMO) MC design and implement these algorithms on a testbed for real-time evaluation. Their analysis is based on the consideration of inter-link interference (ILI) and inter-symbol interference (ISI) for the MIMO design, which are two of the main challenges faced by MCvD systems. Index modulation-based transmission for MCvD systems is introduced in [24], where several modulation schemes are proposed for the mitigation of ISI and ILI. Space-time equalization algorithms are then introduced for further combating ISI and ILI, leading to significant improvement in the performance of MIMO systems and low detection complexity [25].

B. Our Contribution

Inspired by such RF communication systems, we propose a novel molecular beamforming scheme that aims to improve the actuation accuracy in MC networks. From a signal processing perspective, beamforming is defined as a technique used for *directing* a signal towards a particular receiving node [26]. The main benefit of beamforming in RF is the enhancement of the network performance by boosting the signal quality in the intended direction. This is achieved by appropriately delaying transmitted signal components.

Similar to this concept, the proposed idea for cooperative MC is based on the superposition of delayed signal components such that a stronger overall signal is received at the receiver node. Although the concept of cooperative MC has been already investigated in the literature, this work proposes a novel topology resembling to the main concept behind beamforming in wireless communication systems. Moreover, this work focuses on several aspects and approaches towards the reduction of the actuation error rate. This topology can find application in improving the actuation accuracy of MC networks, for which, sensing errors are probable. Let us assume that several sensors have to monitor and stabilize the sugar level of a patient with diabetes. According to the collected information, the duty of these sensors is to initialize a request for an insulin pump when deemed necessary. The main motivation behind this study relies on the idea that as individual sensors are prone to sensing errors, a network which consists of a larger number of sensors will result in having an overall higher accuracy level. From a communication system's perspective, let us assume that the aforementioned scheme incorporates several sensors and two spherical receiver nodes, the actuators (the proposed idea can be easily extended to more than two receivers). It is noteworthy to mention that the actuators are supposed to perform different functions, which are actually application-specific. These sensors are transmitter nodes that emit molecules in accordance with the information they have, with the purpose of activating one receiver at a time, i.e., they collectively target activating one actuator or the other one. A sensing error in the aforementioned scenario could be that the sensors do not activate the node that holds the insulin, when needed. We claim that, given that each sensor senses incorrectly with a probability of error p, the actuation error rate of the overall system decreases if the number of utilized sensors is increased. Molecular beamforming is introduced such that emissions from different sensors are delayed and their respective strengths are adjusted (by controlling the number of emitted molecules from each node), in order for the received signal to be strong enough and decoded with minimum error probability.

In order to validate the proposed system, an analytical approach is followed for demonstrating the impact on the actuation accuracy. Two different error sources are introduced, which are referred to as the activation and deactivation errors.

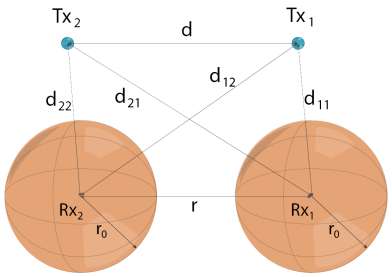

Fig. 1. The generic ULA system that consists of two transmitters (blue spheres) and two receivers (orange spheres). The coordinates of Tx_1, Tx_2, Rx_1, and Rx_2 are [10,0,10.5], [10,0,-10.5], [0,0,10], and [0,0,-10] respectively (in μm), where r_o is 5 μm.

The former occurs when the intended receiver node is not activated, and the latter results from the activation of the non-intended receiver node. Three different scenarios are studied; the first and second scenarios examine the impact of molecular beamforming on the activation error, and the third one takes into consideration both error sources. For the first two scenarios, the error rate in case of a pre-defined threshold at the receiver nodes is examined, and then it is assumed that these nodes can communicate with each other to decide which one will be activated. As expected, the second scenario can achieve better performance, which comes at the cost of increased system complexity due to the need for coordination among the two actuators.

The main contributions of this work are:

- the design of a novel system inspired by beamforming used for actuation in MC networks,
- analysis of the topology for which the transmitters form a uniform linear array (ULA) for understanding the impact of the proposed system in terms of actuation accuracy,
- analysis of a random topology for providing insight into a more practical scenario,
- presentation of analytical and simulation results for the actuation error probability.

The remainder of this paper is organized as follows. In Section II, the ULA and random topologies are introduced, alongside some key design characteristics. Three different scenarios are described in Section III, followed by the actuation error probability analytical derivation. In Section IV, the overall results obtained from this study are discussed. Finally, the conclusion of this paper and future studies are summarized in Section V.

II. System Model

In this section, the proposed system model is presented. As aforementioned, the proposed system consists of several transmitting sensors and two receiving actuator nodes. We first introduce the topology in which the transmitters form a ULA, and then a more realistic one is presented, where the transmitters/sensors are randomly located. Throughout this study, some key design characteristics are followed, which are introduced in this section.

A. ULA Topology

Fig. 1 illustrates a simplified scenario for the topology and forms a basis for the discussion in this section. As in the majority of analytical works in the MC literature, we assume the transmitters to be point sources. The blue spheres are two point transmitters, and the orange spheres are two spherical receivers with equal radii r_o. The distances between the transmitters and the centers of the receivers are denoted by d_{ij}, where i stands for the transmitter and j for the receiver indices, respectively. In this case, we have two of each type of nodes, and due to symmetry, $d_{11} = d_{22}$ and $d_{12} = d_{21}$. The main idea is that we would like to have one of the receivers/actuators to be active at a time, and it is the transmitters' task to emit molecules such that they achieve this activation. In the literature, the single-input-single-output (SISO) topology of an MCvD system is well-studied, and the analytical basis of the channel characteristics for a point transmitter and absorbing spherical receiver is given in [27]. However, in our proposed scenario, each emission from a transmitter constitutes a single-input-multiple-output (SIMO) topology. The analytical foundation for this case is given in [28], and the approximations provided will come of use for the proposed actuation error rate modelling. It is noteworthy to mention that throughout the paper, it is assumed that the channel characteristics are made known to the transmitters, which is the case in most molecular MIMO works in the literature. Whether they emit or not depends on the information that they sense in the surrounding environment.

As seen from Fig. 1, Transmitter 1 (Tx_1) is closer to Receiver 1 (Rx_1), so the number of the received molecules arriving from it is indeed higher compared to that arriving from Transmitter 2 (Tx_2) to Rx_1. In other words, it is expected that if both transmitters are emitting the same number of molecules, then Rx_1 will receive a bigger fraction from Tx_1 compared to Tx_2. As a result, if Rx_1 is the intended receiver to be activated and Tx_2 is emitting, a large fraction of the molecules transmitted by Tx_2 will arrive at Rx_2. If the receiver is activated when the number of received molecules exceeds a threshold value, then this would definitely cause an actuation error. Even if lower power is allocated to the further transmitter, its contribution will not be effective since the further transmitter contributes more molecules to the non-intended receiver. For this reason, it is chosen to ideally allow the transmitters to emit only when their effect is constructive to the intended receiver, not to the other one. Basically, for the topology shown in Fig. 1, Tx_1 will only emit when Rx_1 is the intended receiver to be activated. On the other hand, the second transmitter will only emit when Rx_2 is the intended receiver.

The actuation decision at the receiver side is done based on a comparison between the number of received molecules and a threshold value. To this end, we propose to count the molecules received over an interval of length τ around the peak, $[t_p-\frac{\tau}{2}, t_p+\frac{\tau}{2}]$, where t_p is the peak time. Let us denote the number of molecules received around the peak by Rx_j as $N_{Rx_j}[t_p-\frac{\tau}{2}, t_p+\frac{\tau}{2}]$, which in fact denotes the received signal. Assuming that Rx_1 is to be activated and that both transmitters are sensing correctly, the received overall signal would consist of one component only, the component transmitted from Tx_1. In other words, if the messages from both transmitters are annotated as m_1 and m_2, the ideal case for activating Rx_1 would be $(m_1,m_2) = (1, 0)$, where m_i corresponds to the

TABLE I
PROBABILITY TABLE OF THE EMISSIONS FROM THE TRANSMITTERS RELATED TO THE SENSING ERROR p FOR THE TOPOLOGY WITH TWO TRANSMITTERS

(m_1, m_2)	Probability
$(1,0)$	$(1-p)^2$
$(0,1)$	p^2
$(1,1)$	$p(1-p)$
$(0,0)$	$p(1-p)$

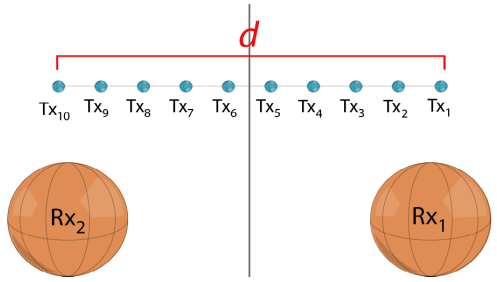

Fig. 2. The proposed ULA system that consists of ten transmitters (blue spheres) and two receivers (orange spheres).

case where Tx_i transmits molecules. In other words, $m_1 = 1$ denotes that Tx_1 is emitting, whereas $m_1 = 0$ denotes that Tx_1 is silent. Due to the sensing error, the transmitters may try to actuate incorrect receivers. The respective probabilities of the four possible cases of the number of received molecules around the peak depending on the emissions from the transmitters, denoted by $N_{Rx_1}[t_p-\frac{\tau}{2}, t_p+\frac{\tau}{2}](m_1, m_2)$, are given in Table I. This table is shown for the case when Rx_1 is to be activated. The sensing error probability is denoted by p. The table is only shown for $N_{Rx_1}[t_p-\frac{\tau}{2}, t_p+\frac{\tau}{2}]$, but a similar logic can be followed for $N_{Rx_2}[t_p-\frac{\tau}{2}, t_p+\frac{\tau}{2}]$ as well.

Up to this point, the system consisting of two transmitters has been discussed. The cases when the number of transmitters is increased should be actually considered. Fig. 2 illustrates the proposed system consisting of ten point transmitters forming a ULA, while keeping d from Tx_1 to Tx_{10} unchanged, and two spherical receivers, as before. In this case, if Rx_1 is to be activated, the transmit nodes from Tx_1 to Tx_5 are ideally turned on and the rest are off; so the overall received signal consists of six components. It is proposed that the different emissions are delayed such that their peaks almost overlap at the receiver node. To do so, the peak time of each component can be calculated beforehand and the delay times can be arranged in such a way that each component's peak overlaps with the latest peak.

Moreover, since these transmitters may be on/off due to a sensing error, it is only fair to allow them to contribute the same level to the received signal. If not, a transmitter with a strong communication channel can easily cause an actuation error if it senses incorrectly. Thus, a power normalization technique is proposed, which corresponds to arranging the number of emitted molecules from each transmitter in advance. This is performed by computing the area under the hitting rate curves of each component for τ seconds around the peak, and adjusting the number of emitted molecules such that all the computed integrals for an activation are equal to each-other.

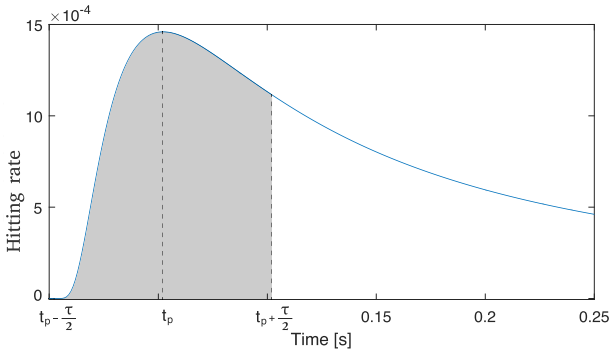

Fig. 3. Computation of I_1 for component received at Rx_1 when Tx_1 is emitting in the ULA topology with $K = 2$ transmitters.

The hitting rate curves of each of the components are obtained as in [28].

To sum up, several key design characteristics are proposed in order to be able to benefit from molecular beamforming in actuation accuracy in MC networks. First of all, the transmitters are ideally on or off, depending on their contribution towards the actuation of the receiving nodes. Secondly, transmitters emit with some pre-defined delay time, in order for the components to arrive almost simultaneously at the receiver side, such that an overall stronger signal is received. Lastly, power normalization is performed before emission by adjusting the number of emitted molecules from each transmitter such that they contribute the same fraction of molecules around the peak. In the following sections, the actuation error rate is computed for the ULA topology with $2K$ transmitters, where $K = 1, 2, 3, 4, 5$, and it is shown that as K increases, so does the actuation accuracy. In Fig. 2, a hypothetical line which passes from $\frac{d}{2}$ is drawn in order to illustrate which transmitters will be on for each activation. The coordinates of the nanomachines used in this study for $K = 1$ are given in Fig. 1.

As for the cases when $K > 1$, the coordinates can be easily computed knowing that d is kept unchanged and the transmitters are equally spaced. The roughly estimated peak times, areas under the hitting rate curves and adjusted number of molecules emitted from each transmitter are shown in Table II for $K = 2$ as an illustration of the explained design steps. In Table II, t_{p_1} and t_{p_2} are the estimated peak times of the molecules received from Tx_i at Rx_1 and Rx_2, respectively. Afterwards, the area under the hitting rate curves for τ seconds around these peaks are computed, given as I_1 and I_2. An example of I_1 computation for the molecules arriving at Rx_1 from Tx_1 is shown in Fig. 3. The shaded area corresponds to the fraction of received molecules during the $[t_p-\frac{\tau}{2}, t_p+\frac{\tau}{2}]$ interval. Referring to Table II, Tx_1 is clearly in favor of Rx_1, thus it will be emitting when Rx_1 is to be activated and it will be turned off for the actuation of Rx_2. As explained above, the number of emitting molecules is adjusted such that each "on" transmitter contributes the same amount of molecules to the overall received signal, given as M_{Rx_1} and M_{Rx_2} in the table. In this study, each transmitter is contributing 1000 molecules around the peak. In other words, the value of I_1 for the component shown in Fig. 3 when Tx_1 is emitting $M_{Rx_1} = 1.05e4$ molecules is 1000. Moreover, the

TABLE II
THE ESTIMATED PARAMETERS OF THE ULA TOPOLOGY WITH $K = 2$ TRANSMITTERS

Tx_i	t_{p_1}	t_{p_2}	I_1	I_2	M_{Rx_1}	M_{Rx_2}	ϕ_1	ϕ_2
Tx_1	$0.055s$	$0.55s$	0.095	0.003	$1.05e4$	–	$0.495s$	$0s$
Tx_2	$0.1s$	$0.295s$	0.053	0.0137	$1.9e4$	–	$0.45s$	$0.255s$
Tx_3	$0.295s$	$0.1s$	0.0137	0.053	–	$1.9e4$	$0.255s$	$0.45s$
Tx_4	$0.55s$	$0.055s$	0.003	0.095	–	$1.05e4$	$0s$	$0.495s$

peak times are different for each component, as expected. The delay times of each emission are computed based on these peak times, denoted by ϕ_1 and ϕ_2 in Table II for the activation of Rx_1 and Rx_2. For the activation of Rx_1, the peak occurring the latest is that of the emission from Tx_4, thus all the other transmitters emit with $\phi_1 = 0.55 - t_{p_1}$ seconds delay. It is noteworthy to mention that all the transmitters should be taken into account in this step, because although Tx_3 and Tx_4 would be ideally off, sensing errors are probable and there is a non-zero probability that they also emit molecules. The symmetry of the ULA cases is also clearly shown by this table.

These steps are illustrated in Fig. 4 for the activation of Rx_1 for the ULA topology of $K = 2$ transmitters. Here, Δt denotes the time step for the update in the particles' locations. Due to symmetry, the same idea would follow for the activation of Rx_2. In Fig. 4a, the peaks of the four components are illustrated, where component 1 refers to the one arriving from Tx_1 and so on. The computation of ϕ_1 is done with respect to the peak occurring the latest. In Fig. 4b, the overall components are shown, as if all transmitters were emitting at $t = 0$. The summation of all components when their peaks are overlapping is shown in Fig. 4c. It should be noted that only the specific area around the peak constitutes the actual signal, which is later compared with a threshold value in order to make the actuation decision.

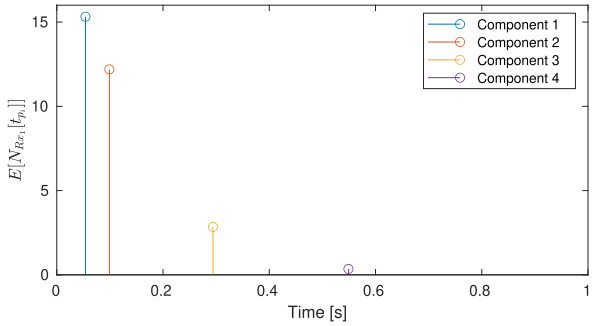

(a)

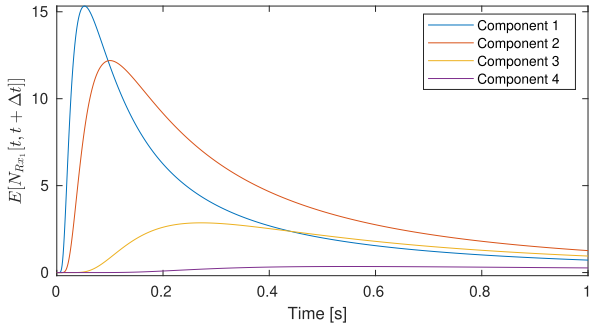

(b)

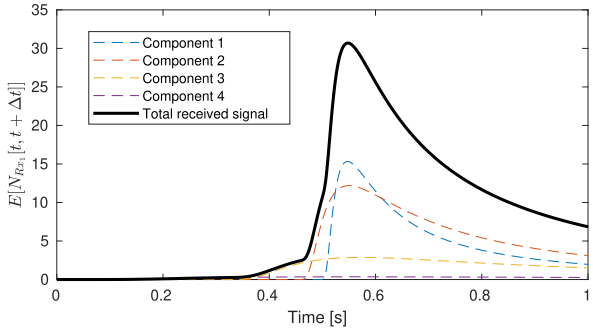

(c)

Fig. 4. ULA topology of $K = 2$ transmitters: (a) The four components at their respective peak times. (b) The overall received components, assuming that all transmitters emit at $t = 0s$. (c) Summation of all components when all transmitters emit at their respective times according to ϕ_1.

B. Random Topology

The ULA case is considered in this work to simplify the concept behind the proposed method. However, transmitters forming a perfect ULA may not be feasible in real life applications. For this reason, a random topology is also presented, such that the transmitters are uniformly and randomly distributed inside a 3-D cuboid, with boundaries ranging from $[-10\ \mu\text{m}, 10\ \mu\text{m}]$. A randomly generated set of coordinates for the $K = 5$ case is given in Fig. 5, such that Tx_1 to Tx_5 are to be on for the activation of Rx_1, while the rest aim the activation of Rx_2. In the following sections, the analytical modelling of the actuation accuracy for different scenarios is given, followed by a comparison between theoretical and simulation results.

III. ACTUATION ACCURACY

In this section, three different scenarios for analysing the actuation accuracy are presented. The proposed scheme may be used in different applications, thus the actuation accuracy may be related to two different kinds of error sources, defined as the activation and deactivation errors. The first one is related to the error occurring as a result of the intended receiver not being activated, whereas the second occurs when the non-intended receiver is mistakenly activated. The impact of molecular beamforming on the activation error is investigated for two different scenarios. In the first scenario, receivers compare the number of molecules received around their individual peaks with a predefined threshold value, which if exceeded, makes the receiver active. In the second scenario, the receivers are assumed to be able to cooperate. They compare their signals and the receiver that has received the larger number of molecules gets actuated. At last, both activation and deactivation errors are examined simultaneously. The analytical formulations for calculating the actuation error are derived for each of the aforementioned cases.

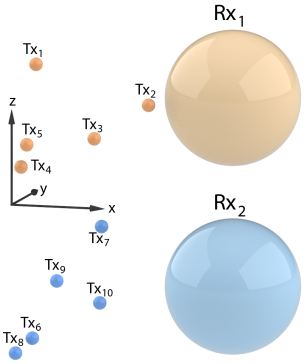

Fig. 5. The random system that consists of ten transmitters and two receivers, where the coordinates of Rx_1, Rx_2 and Tx_1 to Tx_{10} are [7], [10], [14], [14,10,−7], [1], [3], [10], [5], [7], [9], [1], [5], [6], [1,−1,3], [2,-3,5], [3,−5,−9], [4,10,−3], [2,−6,−10], [6,−9,−4] and [5,6,−8], respectively (in μm), where r_o is 5 μm.

A. Predefined Thresholding: Activation Error

The derivation of the activation error rate with predefined threshold values is given for the topology shown in Fig. 1, the two transmitters case. The same idea is followed for the cases when $K > 1$. The cumulative fraction of the molecules emitted from transmitter i and received by receiver j, F_{hit}^{ij}, is computed following the approximations given in [28], given as

$$F_{hit}^{11}(t_d) \cong \frac{r_{o_1}}{d_{11}}\text{erfc}\left(\frac{d_{11}-r_{o_1}}{\sqrt{4\,D\,t_d}}\right) - \frac{r_{o_2}}{d_{12}}\text{erfc}\left(\frac{d_{12}-r_{o_2}}{\sqrt{4\,D\,t_d}}\right) * \frac{r_{o_1}}{r_{v12}}\text{erfc}\left(\frac{r_{v12}-r_{o_1}}{\sqrt{4\,D\,t_d}}\right), \quad (1)$$

$$F_{hit}^{21}(t) \cong \frac{r_{o_1}}{d_{21}}\text{erfc}\left(\frac{d_{21}-r_{o_1}}{\sqrt{4\,D\,t}}\right) - \frac{r_{o_2}}{d_{22}}\text{erfc}\left(\frac{d_{22}-r_{o_2}}{\sqrt{4\,D\,t}}\right) * \frac{r_{o_1}}{r_{v22}}\text{erfc}\left(\frac{r_{v22}-r_{o_1}}{\sqrt{4\,D\,t}}\right), \quad (2)$$

$$F_{hit}^{12}(t) \cong \frac{r_{o_2}}{d_{12}}\text{erfc}\left(\frac{d_{12}-r_{o_2}}{\sqrt{4\,D\,t}}\right) - \frac{r_{o_1}}{d_{11}}\text{erfc}\left(\frac{d_{11}-r_{o_1}}{\sqrt{4\,D\,t}}\right) * \frac{r_{o_2}}{r_{v11}}\text{erfc}\left(\frac{r_{v11}-r_{o_2}}{\sqrt{4\,D\,t}}\right), \quad (3)$$

$$F_{hit}^{22}(t_d) \cong \frac{r_{o_2}}{d_{22}}\text{erfc}\left(\frac{d_{22}-r_{o_2}}{\sqrt{4\,D\,t_d}}\right) - \frac{r_{o_1}}{d_{21}}\text{erfc}\left(\frac{d_{21}-r_{o_1}}{\sqrt{4\,D\,t_d}}\right) * \frac{r_{o_2}}{r_{v21}}\text{erfc}\left(\frac{r_{v21}-r_{o_2}}{\sqrt{4\,D\,t_d}}\right), \quad (4)$$

where r_{vij} denotes the virtual release point from the $i-th$ transmitter to the $j-th$ receiver and D is the diffusion coefficient that depends on the utilized fluid environment and the properties of the molecules. The virtual release point, as denoted in [28], refers to the closest point of the $j-th$ receiver to the $i-th$ transmitter, from where the absorbed molecules would be assumed to be released if they had not been absorbed by the receiver. As discussed earlier, the transmitters emit with some delay in order for these components to arrive almost simultaneously at the receiver side. By observing the peaks of the separate components, the delay is computed such that each component arrives in accordance with the one whose peak occurs the last. As a result, the time is indexed differently for $F_{hit}^{11}(t_d)$ and $F_{hit}^{22}(t_d)$, showing that these components are delayed. The expected number of molecules around the peak of Rx_1 can be computed as a function of m_1 and m_2, as

$$\begin{aligned} &E\left[N_{Rx_1}[t_p-\frac{\tau}{2},t_p+\frac{\tau}{2}](m_1,m_2)\right] \\ &\cong m_1 \times M_{Tx} \times \left(F_{hit}^{11}(t_p+\frac{\tau}{2}) - F_{hit}^{11}(t_p-\frac{\tau}{2})\right) \\ &\quad + m_2 \times M_{Tx} \times \left(F_{hit}^{21}(t_p+\frac{\tau}{2}) - F_{hit}^{21}(t_p-\frac{\tau}{2})\right), \end{aligned} \quad (5)$$

where M_{Tx} is the number of molecules emitted from each transmitter. The signal is obtained as the difference between the two cumulative fractions at times $(t_p+\frac{\tau}{2})$ and $(t_p-\frac{\tau}{2})$, respectively. Due to the symmetry of this topology, if on, each transmitter emits the same number of molecules. As an example, the expected number of molecules around the peak of the components received in Rx_1 for the ideal case is

$$\begin{aligned} &E[N_{Rx_1}[t_p-\frac{\tau}{2},t_p+\frac{\tau}{2}](1,0)] \\ &\quad \cong M_{Tx} \times \left(F_{hit}^{11}(t_p+\frac{\tau}{2}) - F_{hit}^{11}(t_p-\frac{\tau}{2})\right), \end{aligned} \quad (6)$$

which helps us in modeling $N_{Rx_1}[t_p-\frac{\tau}{2},t_p+\frac{\tau}{2}]$ as

$$N_{Rx_1}[t_p-\frac{\tau}{2},t_p+\frac{\tau}{2}](1,0) \sim B(M_{Tx},\, p_{peak,\tau}^{11}). \quad (7)$$

Each molecule arrives at the receiver around the peak with a probability of $p_{peak,\tau}^{11} = \left(F_{hit}^{11}(t_p+\frac{\tau}{2}) - F_{hit}^{11}(t_p-\frac{\tau}{2})\right)$. Here, $p_{peak,\tau}^{11}$ is the success probability of the Binomial distribution with M_{Tx} trials, given that the transmitters are emitting M_{Tx} molecules. Since the Binomial distribution is difficult to work with, as proposed in [29], the Gaussian approximation is used to model (6) as

$$\begin{aligned} &N_{Rx_1}[t_p-\frac{\tau}{2},t_p+\frac{\tau}{2}](1,0) \\ &\sim \mathcal{N}\left(M_{Tx} \times p_{peak,\tau}^{11};\, M_{Tx} \times p_{peak,\tau}^{11} \times (1-p_{peak,\tau}^{11})\right). \end{aligned} \quad (8)$$

The same idea is followed for the other three cases. As an error occurs when the number of received molecules is smaller that the predefined threshold values, the probability of error is computed as

$$\begin{aligned} &P(err) \\ &= P\left(N_{Rx_1}[t_p-\frac{\tau}{2},t_p+\frac{\tau}{2}](m_1,m_2) < \gamma_1 | A=1\right) \\ &\quad \times P(A=1) \\ &\quad + P\left(N_{Rx_2}[t_p-\frac{\tau}{2},t_p+\frac{\tau}{2}](m_1,m_2) < \gamma_2 | A=2\right) \\ &\quad \times P(A=2), \end{aligned} \quad (9)$$

where γ_1 and γ_2 are the predefined thresholds, which are equal due to the symmetry of the scheme, thus $\gamma_1 = \gamma_2 = \gamma$. $A = 1$

denotes the event that Rx_1 is to be activated. Consequently, $P(A=1)=P(A=2)=\frac{1}{2}$ in the simulations, resulting in

$$P(err)=\frac{1}{2}\Big[P\left(N_{Rx_1}[t_p-\frac{\tau}{2},t_p+\frac{\tau}{2}](m_1,m_2)<\gamma|A=1\right)+P\left(N_{Rx_2}[t_p-\frac{\tau}{2},t_p+\frac{\tau}{2}](m_1,m_2)<\gamma|A=2\right)\Big]. \tag{10}$$

The components in (10) are equal to each other, so the probability of error can be finally expressed as

$$P(err)=P\left(N_{Rx_1}[t_p-\frac{\tau}{2},t_p+\frac{\tau}{2}](m_1,m_2)<\gamma|A=1\right). \tag{11}$$

From the Gaussian approximations above, the probability of error by using the $Q(.)$ function can be computed in the form

$$P\big(N_{Rx_1}[t_p-\frac{\tau}{2},t_p+\frac{\tau}{2}](1,0)<\gamma|A=1\big)=(1-p)^2\times Q\left(\frac{M_{Tx}\times p^{11}_{peak,\tau}-\gamma}{\sqrt{M_{Tx}\times p^{11}_{peak,\tau}\times(1-p^{11}_{peak,\tau})}}\right), \tag{12}$$

where $Q(.)$ function is the tail distribution function of the normal distribution. Then, the probability of error is analytically computed by summing up the error as a result of the four cases. The same process is followed for the cases of $K>1$.

B. Mutual Thresholding: Activation Error

Unlike the predefined thresholding case, the decision whether a receiver is active or not is done based on the comparison of the signal between the two receivers. As expected, the complexity is increased for this scenario, since it requires a communication channel between the two receiving nodes. Following a similar approach as before, the error probability for the two transmitters case can be computed by

$$P(err)=P\Big(N_{Rx_1}[t_p-\frac{\tau}{2},t_p+\frac{\tau}{2}](m_1,m_2)<N_{Rx_2}[t_p-\frac{\tau}{2},t_p+\frac{\tau}{2}](m_1,m_2)|A=1\Big), \tag{13}$$

$$P(err)=P\Big(N_{Rx_1}[t_p-\frac{\tau}{2},t_p+\frac{\tau}{2}](m_1,m_2)-N_{Rx_2}[t_p-\frac{\tau}{2},t_p+\frac{\tau}{2}](m_1,m_2)<0|A=1\Big). \tag{14}$$

Since the reception events are independent, the distribution of $N_{Rx_1}[t_p-\frac{\tau}{2},t_p+\frac{\tau}{2}](m_1,m_2)-N_{Rx_2}[t_p-\frac{\tau}{2},t_p+\frac{\tau}{2}](m_1,m_2)$ random variable can be given as

$$N_{Rx_1}[t_p-\frac{\tau}{2},t_p+\frac{\tau}{2}](m_1,m_2)-N_{Rx_2}[t_p-\frac{\tau}{2},t_p+\frac{\tau}{2}](m_1,m_2)\sim\mathcal{N}\Big(\mu_{N_{Rx_1}[t_p-\frac{\tau}{2},t_p+\frac{\tau}{2}](m_1,m_2)}-\mu_{N_{Rx_2}[t_p-\frac{\tau}{2},t_p+\frac{\tau}{2}](m_1,m_2)},\times\sigma^2_{N_{Rx_1}[t_p-\frac{\tau}{2},t_p+\frac{\tau}{2}](m_1,m_2)}+\sigma^2_{N_{Rx_2}[t_p-\frac{\tau}{2},t_p+\frac{\tau}{2}](m_1,m_2)}\Big), \tag{15}$$

where $\mu_{N_{Rx_1}[t_p-\frac{\tau}{2},t_p+\frac{\tau}{2}](m_1,m_2)}$ and $\mu_{N_{Rx_2}[t_p-\frac{\tau}{2},t_p+\frac{\tau}{2}](m_1,m_2)}$ are the respective means of $N_{Rx_1}[t_p-\frac{\tau}{2},t_p+\frac{\tau}{2}]$ and $N_{Rx_2}[t_p-\frac{\tau}{2},t_p+\frac{\tau}{2}]$, and $\sigma^2_{N_{Rx_1}[t_p-\frac{\tau}{2},t_p+\frac{\tau}{2}](m_1,m_2)}$ and $\sigma^2_{N_{Rx_2}[t_p-\frac{\tau}{2},t_p+\frac{\tau}{2}](m_1,m_2)}$ are their variances, respectively. The activation error can then be analytically computed.

C. Composite Error

In the aforementioned cases, no error is encountered as long as the intended receiver is activated. However, in some applications, the system designer may want to make sure that only the intended receiver must be active. In this case, when both receivers are active given that only one is intended may count towards an error. Therefore, we can consider the total error to consist of both activation and deactivation error sources and call this case the composite error case. The probability of correct actuation is given as

$$P(c)=\frac{1}{2}\Big[P\Big(N_{Rx_1}[t_p-\frac{\tau}{2},t_p+\frac{\tau}{2}](m_1,m_2)>\gamma\wedge\times N_{Rx_2}[t_p-\frac{\tau}{2},t_p+\frac{\tau}{2}](m_1,m_2)<\gamma|A=1\Big)+P\Big(N_{Rx_2}[t_p-\frac{\tau}{2},t_p+\frac{\tau}{2}](m_1,m_2)>\gamma\wedge\times N_{Rx_1}[t_p-\frac{\tau}{2},t_p+\frac{\tau}{2}](m_1,m_2)<\gamma|A=2\Big)\Big]. \tag{16}$$

Due to the symmetry of the scheme and the independence of the two reception events, the error probability can then be computed as

$$P(err)=1-P\left(N_{Rx_1}[t_p-\frac{\tau}{2},t_p+\frac{\tau}{2}](m_1,m_2)>\gamma|A=1\right)\times P\left(N_{Rx_2}[t_p-\frac{\tau}{2},t_p+\frac{\tau}{2}](m_1,m_2)<\gamma|A=1\right). \tag{17}$$

As an example, shown for the $(m_1,m_2)=(1,0)$, the error probability can be computed as

$$P\left(N_{Rx_1}[t_p-\frac{\tau}{2},t_p+\frac{\tau}{2}](1,0)<\gamma|A=1\right)\times P\left(N_{Rx_2}[t_p-\frac{\tau}{2},t_p+\frac{\tau}{2}](1,0)>\gamma|A=1\right)=(1-p)^2\times Q\left(\frac{\gamma-\mu_{Rx_{1_{peak}(1,0)}}}{\sigma_{N_{Rx_1}[t_p-\frac{\tau}{2},t_p+\frac{\tau}{2}](1,0)}}\right)\times Q\left(\frac{\mu_{Rx_{2_{peak}(1,0)}}-\gamma}{\sigma_{N_{Rx_2}[t_p-\frac{\tau}{2},t_p+\frac{\tau}{2}](1,0)}}\right). \tag{18}$$

The threshold value γ can be optimized for this case, such that the probability of error reaches a minimum. The overall results of the predefined thresholding, mutual thresholding, and the composite error case are presented in the following section.

IV. Simulation Results

The validation of the proposed scheme is done by comparing the analytical results following the derivations done in Section III with the results obtained from particle-based simulations. The transmitters are assumed to correctly sense

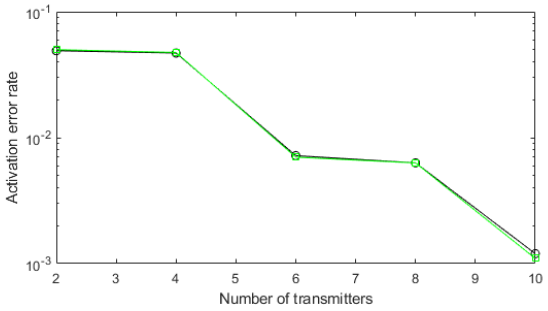

Fig. 6. The analytical and simulation results for the predefined thresholding scenario of the ULA topology.

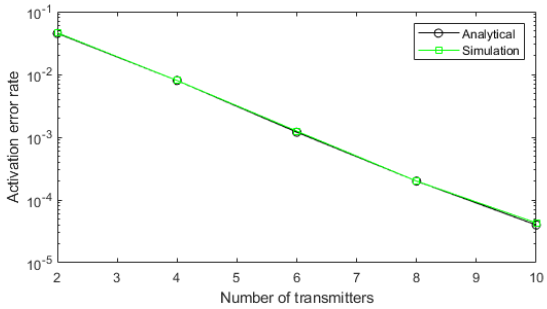

Fig. 7. The analytical and simulation results for the mutual thresholding scenario of the ULA topology.

for 95% of the time, such that $p = 0.05$. The peak times of the received components are roughly estimated from their hitting rate curves. The window size around the peak is selected as $\tau = 0.1\ s$. As for the power normalization procedure previously explained, the number of molecules emitted is adjusted such that each transmitter for each case contributes 1000 molecules around the peak of the overall received signal. The simulation results for computing the actuation errors are obtained for 10^3 actuations, such that a random array containing information of which receiver is to be activated is generated with size 10^3, and the error rate is computed at the end of the simulation. The time step size Δt is 10^{-3} s. The value of diffusion coefficient D is taken as $79.4\mu m^2/s$ throughout the simulations, whereas r_o is always 5 μm.

The threshold value for the topology with two transmitters with the predefined thresholding scenario is selected as $\gamma = \frac{E[N_{Rx_1}[t_p-\frac{\tau}{2},t_p+\frac{\tau}{2}](1,0)]+E[N_{Rx_1}[t_p-\frac{\tau}{2},t_p+\frac{\tau}{2}](0,0)]}{2}$. The same idea is followed for $K > 1$, where the first term in the threshold value represents the ideal case. In other words, the threshold values are $\gamma_K = 500, 1000, 1500, 2000, 2500$ for $K = 1, 2, 3, 4, 5$. As can be seen from Fig. 6, the simulation results fit the analytical ones almost perfectly. As expected, the activation error rate drops down to 10^{-3} for $K = 5$. Moreover, an interesting behavior can be observed from these curves. The activation error rate drops following a staircase-like shape. The accuracy is observed to be higher for odd values of K, compared to even values. This can be explained by considering the activation of a receiver as a decision done by the transmitters, so, when K is odd, the result of their "majority vote" is more apparent. In other words, an odd value of K leads to a lower probability of a "tie" between the on and off transmitters, even in the case of sensing errors.

The results for the mutual-thresholding case are provided in Fig. 7. There is a clear improvement in the activation error rate, compared with the results presented earlier. This comes at the cost of assuming a perfect communication channel between the receivers such that they co-decide which one is to be activated. As a result, it can be said that there exists a trade-off between the system's complexity and the overall achieved accuracy.

The threshold value for the composite error scenario is a key parameter, because a low value would reduce the activation error while causing the deactivation error to increase, and a high value would do the opposite. In order to minimize the overall error, the optimized γ is found numerically as the value for which (17) reaches a minimum. The analytical results are compared with simulation results, and the overall composite error rate curves are shown in Fig. 8. The γ values used in the simulations are $\gamma_K = 490, 650, 1750, 1940, 2900$ for $K = 1, 2, 3, 4, 5$, respectively. Similar to the behavior of the curves in Fig. 6, it can be concluded that an odd value of K ensures a better performance for the composite error case, as it enables the scheme to be less prone to the deactivation error.

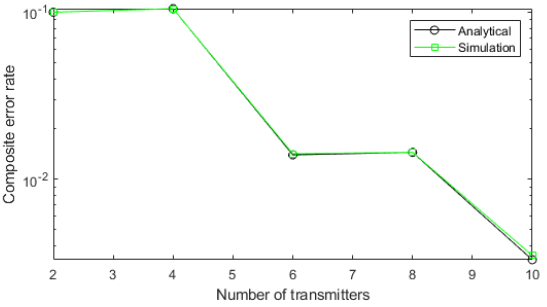

Fig. 8. The analytical and simulation results for the composite error scenario of the ULA topology.

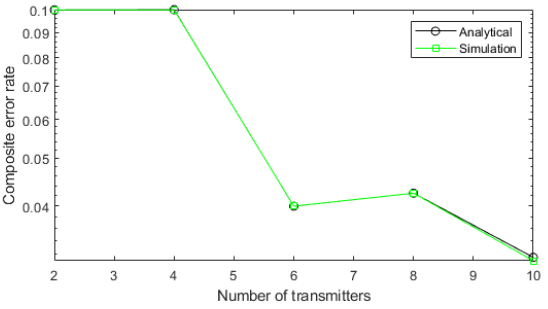

Fig. 9. The analytical and simulation results for the composite error scenario of the random topology.

Lastly, the results of the composite error scenario for the random topology presented in the previous sections are provided. As it is shown in Fig. 9, the performance of the random topology has similar characteristics with the ULA topology. The optimized γ values are $\gamma_K = 430, 780, 1940, 2825, 3760$ for $K = 1, 2, 3, 4, 5$, respectively.

It is noteworthy to mention that allocating all the power to the closest transmitter to the intended receiver performs worse, since the accuracy actually increases when the sensors take the actuation decision altogether. Even if all the sensors are used for an activation the performance is worse, since in that case, an error is more probable due to the possible emissions from the non-contributing sensors.

V. Conclusion

In this work, a novel molecular beamforming design has been proposed in order to increase the actuation accuracy in MC networks. This design may find application on different tasks related to nano scale medicine and healthcare. The proposed system consists of several transmitting nodes, which, according to the application, aim to activate one receiver at a time. Given that there exists a probability of sensing error, it is claimed that if the number of transmitters is increased, the actuation accuracy is improved. The goal is to improve the quality of the signal received at the intended receiver, and to do so, there are several design characteristics followed throughout the study. First, given the node that has to be active, a transmitter has to emit or stay quiet, based on whether its contribution to that node's received signal is constructive or not. Secondly, the transmitters emit with a predefined delay time, such that the peaks of the received components almost overlap at the receiver. Moreover, since errors may occur, the number of emitted molecules is adjusted beforehand, in order for each transmitter to contribute the same towards the activation of the receiver node. This is because of the case in which the transmitter which contributes the most stays quiet by mistake and the probability of an actuation error to occur is higher.

The proposed design is validated both analytically and by means of computer simulations. Three different scenarios for computing the actuation error are presented, and the analytical derivation is provided for each. The ULA placement of transmitters is presented first for simplifying the concept of beamforming. A more realistic scenario is presented as well. It has been concluded that there exists a trade-off between the actuation accuracy and system's complexity. Moreover, the system performs better when the number of transmitters used to activate a receiver node is odd.

As this is, to the best of our knowledge, a pioneering work on molecular beamforming, future works may focus on further optimizing this system and its parameters. Such optimization may include γ, τ, and the contribution of molecules from each transmitter around the peak. Moreover, further improvement may be done in regard to the computation of the peak times, as in this study, they are roughly estimated.

References

[1] I. F. Akyildiz, F. Brunetti, and C. Blázquez, "Nanonetworks: A new communication paradigm," *Comput. Netw.*, vol. 52, no. 12, pp. 2260–2279, Aug. 2008.

[2] T. Nakano, M. J. Moore, F. Wei, A. V. Vasilakos, and J. Shuai, "Molecular communication and networking: Opportunities and challenges," *IEEE Trans. Nanobiosci.*, vol. 11, no. 2, pp. 135–148, Jun. 2012.

[3] T. Nakano, A. W. Eckford, and T. Haraguchi, *Molecular Communication*. Cambridge, U.K.: Cambridge Univ. Press, Sep. 2013.

[4] Q. H. Abbasi et al., "Nano-communication for biomedical applications: A review on the state-of-the-art from physical layers to novel networking concepts," *IEEE Access*, vol. 4, pp. 3920–3935, 2016.

[5] Y. Cevallos, L. Tello-Oquendo, D. Inca, D. Ghose, A. Z. Shirazi, and G. A. Gomez, "Health applications based on molecular communications: A brief review," in *Proc. IEEE Int. Conf. E-Health Netw., Appl. Services (HealthCom)*, Oct. 2019, pp. 1–6.

[6] L. Felicetti, M. Femminella, G. Reali, and P. Liò, "Applications of molecular communications to medicine: A survey," *Nano Commun. Netw.*, vol. 7, pp. 27–45, Mar. 2016.

[7] G. Reali, M. Femminella, L. Felicetti, and P. Liò, "Endovascular mobile sensor network for detecting circulating tumoral cells," in *Proc. 9th Int. Conf. Body Area Netw.*, Sep. 2014, pp. 111–117.

[8] Y. Chahibi, M. Pierobon, S. O. Song, and I. F. Akyildiz, "A molecular communication system model for particulate drug delivery systems," *IEEE Trans. Biomed. Eng.*, vol. 60, no. 12, pp. 3468–3483, Dec. 2013.

[9] U. Chude-Okonkwo, R. Malekian, and B. T. Maharaj, *Advanced Targeted Nanomedicine*. Cham, Switzerland: Springer, 2019.

[10] R. M. DiSanto, V. Subramanian, and Z. Gu, "Recent advances in nanotechnology for diabetes treatment," *Wiley Interdiscipl. Rev., Nanomed. Nanobiotechnol.*, vol. 7, no. 4, pp. 548–564, Jul. 2015.

[11] S. Shitharth, P. Meshram, P. R. Kshirsagar, H. Manoharan, V. Tirth, and V. P. Sundramurthy, "Impact of big data analysis on nanosensors for applied sciences using neural networks," *J. Nanomater.*, vol. 2021, pp. 1–9, Sep. 2021.

[12] M. Aloraefy, T. Pfefer, J. Ramella-Roman, and K. Sapsford, "In vitro evaluation of fluorescence glucose biosensor response," *Sensors*, vol. 14, no. 7, pp. 12127–12148, Jul. 2014.

[13] *In Vitro Diagnostic Test Systems: Requirements for Blood-Glucose Monitoring Systems for Self-Testing in Managing Diabetes Mellitus*, Int. Org. Standardization, Geneva, Switzerland, 2003.

[14] F. Aberer et al., "Accuracy and stability of an arterial sensor for glucose monitoring in a porcine model using glucose clamp technique," *Sci. Rep.*, vol. 10, no. 1, pp. 1–9, Apr. 2020.

[15] N. Agoulmine, K. Kim, S. Kim, T. Rim, J. Lee, and M. Meyyappan, "Enabling communication and cooperation in bio-nanosensor networks: Toward innovative healthcare solutions," *IEEE Wireless Commun.*, vol. 19, no. 5, pp. 42–51, Oct. 2012.

[16] L. Khaloopour, M. Mirmohseni, and M. Nasiri-Kenari, "Theoretical concept study of cooperative abnormality detection and localization in fluidic-medium molecular communication," *IEEE Sensors J.*, vol. 21, no. 15, pp. 17118–17130, Aug. 2021.

[17] R. Mosayebi, W. Wicke, V. Jamali, A. Ahmadzadeh, R. Schober, and M. Nasiri-Kenari, "Advanced target detection via molecular communication," in *Proc. IEEE Global Commun. Conf. (GLOBECOM)*, Dec. 2018, pp. 1–7.

[18] L. Khaloopour, M. Mirmohseni, and M. Nasiri-Kenari, "Joint sensing, communication and localization of a silent abnormality using molecular diffusion," 2022, *arXiv:2203.16641*.

[19] N. Varshney, A. Patel, Y. Deng, W. Haselmayr, P. K. Varshney, and A. Nallanathan, "Abnormality detection inside blood vessels with mobile nanomachines," *IEEE Trans. Mol., Biol. Multi-Scale Commun.*, vol. 4, no. 3, pp. 189–194, Sep. 2018.

[20] R. Mosayebi, A. Ahmadzadeh, W. Wicke, V. Jamali, R. Schober, and M. Nasiri-Kenari, "Early cancer detection in blood vessels using mobile nanosensors," *IEEE Trans. Nanobiosci.*, vol. 18, no. 2, pp. 103–116, Apr. 2019.

[21] S. Ghavami, "Anomaly detection in molecular communications with applications to health monitoring networks," *IEEE Trans. Mol., Biol. Multi-Scale Commun.*, vol. 6, no. 1, pp. 50–59, Jul. 2020.

[22] Y. Fang, A. Noel, N. Yang, A. W. Eckford, and R. A. Kennedy, "Maximum likelihood detection for cooperative molecular communication," in *Proc. IEEE Int. Conf. Commun. (ICC)*, May 2018, pp. 1–7.

[23] B. Koo, C. Lee, H. B. Yilmaz, N. Farsad, A. Eckford, and C. Chae, "Molecular MIMO: From theory to prototype," *IEEE J. Sel. Areas Commun.*, vol. 34, no. 3, pp. 600–614, Mar. 2016.

[24] M. C. Gursoy, E. Basar, A. E. Pusane, and T. Tugcu, "Index modulation for molecular communication via diffusion systems," *IEEE Trans. Commun.*, vol. 67, no. 5, pp. 3337–3350, May 2019.

[25] M. C. Gursoy, A. Celik, E. Basar, A. E. Pusane, and T. Tugcu, "Molecular index modulation with space-time equalization," *IEEE Wireless Commun. Lett.*, vol. 9, no. 5, pp. 702–705, May 2020.

[26] B. D. Van Veen and K. M. Buckley, "Beamforming: A versatile approach to spatial filtering," *IEEE ASSP Mag.*, vol. 5, no. 2, pp. 4–24, Apr. 1988.

[27] H. B. Yilmaz, A. C. Heren, T. Tugcu, and C. Chae, "Three-dimensional channel characteristics for molecular communications with an absorbing receiver," *IEEE Commun. Lett.*, vol. 18, no. 6, pp. 929–932, Jun. 2014.

[28] G. Yaylali, B. C. Akdeniz, T. Tugcu, and A. E. Pusane, "Channel modeling for multi-receiver molecular communication systems," 2021, *arXiv:2111.09302*.

[29] H. B. Yilmaz and C. Chae, "Arrival modelling for molecular communication via diffusion," *Electron. Lett.*, vol. 50, no. 23, pp. 1667–1669, Nov. 2014.